Groupwise multichannel image registration

Guyader, Jean Marie; Huizinga, Wyke; Fortunati, Valerio; Poot, Dirk H.J.; Veenland, Jifke F.; Paulides, Margarethus M.; Niessen, Wiro J.; Klein, Stefan

DOI
10.1109/JBHI.2018.2844361

Publication date
2019

Document Version
Final published version

Published in
IEEE Journal of Biomedical and Health Informatics

Groupwise Multichannel Image Registration

Jean-Marie Guyader, Wyke Huizinga, Valerio Fortunati, Dirk H. J. Poot, Jifke F. Veenland, Margarethus M. Paulides, Wiro J. Niessen, and Stefan Klein

***Abstract*—Multichannel image registration is an important challenge in medical image analysis. Multichannel images result from modalities such as dual-energy CT or multispectral microscopy. Besides, multichannel feature images can be derived from acquired images, for instance, by applying multiscale feature banks to the original images to register. Multichannel registration techniques have been proposed, but most of them are applicable to only two multichannel images at a time. In the present study, we propose to formulate multichannel registration as a groupwise image registration problem. In this way, we derive a method that allows the registration of two or more multichannel images in a fully symmetric manner (i.e., all images play the same role in the registration procedure), and therefore, has transitive consistency by definition. The method that we introduce is applicable to any number of multichannel images, any number of channels per image, and it allows to take into account correlation between any pair of images and not just corresponding channels. In addition, it is fully modular in terms of dissimilarity measure, transformation model, regularisation method, and optimisation strategy. For two multimodal datasets, we computed feature images from the initially acquired images, and applied the proposed registration technique to the newly created sets of multichannel images. MIND descriptors were used as feature images, and we chose total correlation as groupwise dissimilarity measure. Results show that groupwise multichannel image registration is a competitive alternative to the pairwise multichannel scheme, in terms of registration accuracy and insensitivity towards registration reference spaces.**

Manuscript received February 1, 2018; revised May 7, 2018; accepted June 3, 2018. Date of publication June 6, 2018; date of current version May 6, 2019. This work was supported in part by the Innovative Medicines Initiative Joint Undertaking (http://www.imi.europa.eu) under Grant 115151 (QuIC-ConCePT project), which is funded by the European Union's Seventh Framework Programme (FP7/2007-2013) (EU-FP7) and EFPIA companies in kind contribution, and in part by the EU-FP7 under Grant 601055 (VPH-DARE@IT.) *(Corresponding author: Jean-Marie Guyader.)*

J.-M. Guyader, W. Huizinga, V. Fortunati, D. H. J. Poot, J. F. Veenland, and S. Klein are with the Biomedical Imaging Group Rotterdam, Departments of Radiology and Medical Informatics, Erasmus MC Cancer Institute—University Medical Centre Rotterdam, Rotterdam 3000 CA, The Netherlands (e-mail: jeanmarie.guyader@gmail.com; w.huizinga@erasmusmc.nl; v.fortunati@erasmusmc.nl; d.poot@erasmusmc.nl; j.veenland@erasmusmc.nl; s.klein@erasmusmc.nl).

M. M. Paulides is with the Hyperthermia Unit, Department of Radiation Oncology, Erasmus MC Cancer Institute—University Medical Centre Rotterdam, Rotterdam 3000 CA, The Netherlands (e-mail: m.paulides@erasmusmc.nl).

W. J. Niessen is with the Biomedical Imaging Group Rotterdam, Departments of Radiology and Medical Informatics, Erasmus MC Cancer Institute—University Medical Centre Rotterdam, Rotterdam 3000 CA, The Netherlands, and also with the Imaging Science and Technology, Faculty of Applied Sciences, Delft University of Technology, Delft 2628, CD, The Netherlands (e-mail: w.niessen@erasmusmc.nl).

Digital Object Identifier 10.1109/JBHI.2018.2844361

***Index Terms*—Feature images, groupwise image registration, multi-channel registration, dissimilarity measure.**

I. Introduction

IMAGE registration is an important tool for medical image analysis. Medical image datasets can be made up of images obtained from different modalities, time points, or patients, for instance. Spatial correspondence between the images is therefore, in most cases, not naturally ensured. Automated image registration can be used to realign such datasets, which is crucial for many post-acquisition image processing techniques.

Among the large range of image registration techniques that have been developed, various research works have focused on multi-channel registration. Multi-channel image registration consists of applying registration to images for which several channels are available. The channels of a given multi-channel image can be obtained from different post-acquisition operations (e.g. filtering, computation of feature images), or from different acquisitions (e.g. different modalities or time points). In this study, we consider an image as being multi-channel when its channel images are spatially registered, either because they are naturally spatially registered, or thanks to a preliminary registration step. Multi-channel image registration is the task of finding spatial correspondences between several such multi-channel images. Rhode *et al*. [1], [2] were among the first to propose a method handling the registration of two multi-channel images. They designed an approach based on multivariate correlation, and applied it in the context of diffusion-tensor imaging. Other applications of multi-channel registration focus on the registration of feature images: instead of applying registration to the images originally present in a dataset, feature images derived from the original images are used for the registration. Such a technique was proposed by Legg *et al*. [3], who extracted several feature images based on Gaussian derivatives, and subsequently registered these feature images using a dissimilarity measure based on regional mutual information [4]. Staring *et al*. [5] designed α-mutual information, a technique that registers sets of feature images using the concepts of mutual information. Heinrich *et al*. [6] created a registration similarity measure based on a sum of squared absolute differences of the feature images, to register sets of multiple feature images obtained with a descriptor called modality independent neighbourhood descriptor (MIND). Li *et al*. [7] derived another descriptor from MIND, and named it the autocorrelation of local structure (ALOST). Suarez *et al*. [8] used a registration technique based on a dissimilarity measure derived from the correlation matrix

of two multi-channel images. Heinrich *et al*. [9] introduced local canonical correlation analysis, a method that assess dissimilarity into new bases that best represent the relations between two multi-channel images. Chen *et al*. [10] addressed the pairwise registration of two images of different modalities by generating synthetic images that are considered as a second channel for pairwise image registration.

Most multi-channel methods that were previously proposed are pairwise registration schemes. This means that they are applicable to only two multi-channel images at a time, and require to select a fixed reference image to which the remaining multi-channel image will be registered. These multi-channel pairwise registration schemes have the drawback that they require the choice of fixed reference image, which may bias registration accuracy, as shown by Geng *et al*. [11].

In the present study, we propose a novel framework for multi-channel image registration. The key idea is to cast multi-channel registration as a groupwise registration problem. The novel registration technique that we devise is suitable not only for the common case of two multi-channel images, but also for cases in which the aim is to register three or more multi-channel images at a time. The multi-channel registration method that we propose is designed as a groupwise registration problem: it is symmetric and all image data is taken into account simultaneously in a single optimisation procedure.

Various groupwise registration methods have been proposed. One of the earliest groupwise method was the technique of Joshi *et al*. [12], based on unbiased diffeomorphic registration. Learned-Miller [13] presented a groupwise method consisting of minimising the sum of the pixelwise entropies computed at each voxel location. Bhatia *et al*. [14] designed a groupwise dissimilarity measure based on the sum of the entropies of each image. Metz *et al*. [15] proposed a groupwise dissimilarity measure based on voxelwise variance, designed for monomodal images. A few groupwise methods for multimodal images or multiparametric images (i.e. same modality, different acquisition settings) were presented, such as an efficient joint entropy minimisation presented by Spiclin *et al*. [16], a sum of accumulated pairwise estimates presented by Wachinger *et al*. [17], a technique based on principal component analysis introduced by [18], a technique based on Pythagorean means created by Polfliet *et al*. [19], and a technique based on total correlation that we previously proposed [20]. It was not investigated in the literature whether and how these methods could be applicable to multi-channel images.

In this study, the generic groupwise multi-channel registration framework that we propose is applicable to any number of multi-channel images, any number of channels per image, and allows to take into account correlations between any pair of channel images. Moreover, it is fully modular in terms of dissimilarity measure, transformation model, regularisation method and optimisation strategy.

II. Method

A. Preliminaries

Let us consider $\tilde{M}_1, \ldots, \tilde{M}_G$, a series of $G \geq 2$ multi-channel images. One multi-channel image will be denoted $\tilde{M}_g$, and its associated channel images will be denoted $\tilde{M}_{g,f}$ (the index f varies between 1 and the number of channels F_g of image $\tilde{M}_g$). The multi-channel images $\tilde{M}_1, \ldots, \tilde{M}_G$ have $F_1, \ldots, F_G$ channels, respectively. The complete set of image channels to register is therefore:

$$\tilde{\mathcal{M}} = \left\{ \tilde{M}_{g,f} \quad \text{with} \quad g = 1 \cdots G \text{ and } f = 1 \cdots F_g \right\} \tag{1}$$

Each channel image $\tilde{M}_{g,f}$ is associated with a differentiable function $\tilde{M}_{g,f}(\boldsymbol{x})$ of the spatial coordinate $\boldsymbol{x}$.

Multi-channel image registration is the task of finding the spatial correspondence between several misaligned multi-channel images, assuming that the channel images of each multi-channel image are already all aligned. This study focuses on intensity-based registration methods based on the minimisation of a dissimilarity measure $\mathcal{D}$.

For the particular case of mono-channel image registration (i.e. $F_1 = \cdots = F_G = 1$), each image $\tilde{M}_g$ can be assimilated with its single channel image $\tilde{M}_{g,1}$. In that case, the following shorthand notation will be used: $M_g = \tilde{M}_g = \tilde{M}_{g,1}$.

B. Existing Pairwise Multi-Channel Image Registration

All multi-channel registration methods designed so far are pairwise: they are limited to $G = 2$ images and require the selection of a fixed reference space among the multi-channel images to register. Let us consider two multi-channel images $\tilde{M}_1$ and $\tilde{M}_2$. When the numbers of channels F_1 and F_2 are equal ($F_1 = F_2 = F$), a generalized pairwise multi-channel (PMC) dissimilarity measure $\mathcal{D}_{\mathrm{PMC}}$ can be written:

$$\mathcal{D}_{\mathrm{PMC}}(\tilde{\mathcal{M}}) = \sum_{f=1}^{F} \mathcal{D}_{\mathrm{pairwise}} \left(\tilde{M}_{1,f}, \tilde{M}_{2,f} \right) \tag{2}$$

with $\mathcal{D}_{\mathrm{pairwise}}$ a pairwise mono-channel dissimilarity measure that can be chosen among the wide range of pairwise measures conventionally used in image registration such as the sum of squared differences, or mutual information [21]. One multi-channel image is taken as fixed reference (here $\tilde{M}_1$). The other multi-channel image is known as the moving image (here $\tilde{M}_2$). The aim of pairwise multi-channel image registration is to minimise the following function:

$$\hat{\boldsymbol{\mu}} = \arg\min_{\boldsymbol{\mu}} \mathcal{D}_{\mathrm{PMC}}(\tilde{M}_{1,f}(\boldsymbol{x}), \ldots, \tilde{M}_{1,F}(\boldsymbol{x}), \tilde{M}_{2,1}(\boldsymbol{T}(\boldsymbol{x}, \boldsymbol{\mu})), \ldots, \tilde{M}_{2,F}(\boldsymbol{T}(\boldsymbol{x}, \boldsymbol{\mu}))) \tag{3}$$

with $\boldsymbol{T}(\boldsymbol{x}, \boldsymbol{\mu})$ the registration transformation applied to the channels of the moving image $\tilde{M}_{2,1}, \ldots, \tilde{M}_{2,F}$, where $\boldsymbol{\mu}$ is a vector containing the parameters of the transformation, e.g. rotations and translations for a rigid transformation model, or B-spline coefficients for a free-form deformation model [22].

When $G > 2$ initially acquired images are considered, the pairwise multi-channel image registration scheme can still be used, but it should be applied $G - 1$ times. One multi-channel image must be chosen as fixed reference image, e.g. $\tilde{M}_1$, to which the other images are registered. Disadvantages of such a scheme are that each independent registration is performed using only a fraction of the total available image information, and that the registration result depends on the choice of reference image [11].

C. Existing Groupwise Mono-Channel Registration Scheme

Contrary to pairwise registration, groupwise registration allows to register multiple images in one optimisation procedure, without the need to select a fixed image space reference [13], [15]–[18], [23]. The aim of groupwise mono-channel registration is to simultaneously bring the $G \geq 2$ mono-channel images $M_g(\boldsymbol{x})$ of $\tilde{\mathcal{M}}$ to a mid-point space, by means of a transformation $\boldsymbol{T}(\boldsymbol{x}, \boldsymbol{\mu})$, where $\boldsymbol{\mu}$ is a vector containing the parameters $\boldsymbol{\mu}_g$ of the transformation $\boldsymbol{T}_g(\boldsymbol{x}, \boldsymbol{\mu}_g)$ that is applied to each image M_g. Let us denote $\mathcal{D}$ a measure quantifying the dissimilarity between all transformed images $M_g(\boldsymbol{T}_g(\boldsymbol{x}, \boldsymbol{\mu}_g))$. Groupwise mono-channel registration can then be formulated as the minimisation of the dissimilarity measure $\mathcal{D}$ with respect to $\boldsymbol{\mu}$:

$$\hat{\boldsymbol{\mu}} = \arg\min_{\boldsymbol{\mu}} \mathcal{D}(M_1(\boldsymbol{T}_1(\boldsymbol{x}, \boldsymbol{\mu}_1)), \ldots, M_G(\boldsymbol{T}_G(\boldsymbol{x}, \boldsymbol{\mu}_G))) \tag{4}$$

subject to:

$$\sum_{g=1}^{G} \boldsymbol{\mu}_g = \mathbf{0} \tag{5}$$

where the constraint of Equation (5) serves to define a mid-point space [24]. An attractive property of groupwise registrations is that they are fully symmetric (i.e. all images play the same role in the registration procedure), and are transitive consistent by definition.

D. Novel Groupwise Multi-Channel Image Registration

The aim of the novel registration scheme that we propose is to solve multi-channel image registration by treating it as a groupwise registration problem. Simply extending the optimisation scheme presented in Equation 4 to channel images taken as individual images would not be satisfactory. Indeed, this would not take into account the knowledge that some images belong together, while others do not. The multi-channel nature of the images introduces an extra constraint: the channel images $\tilde{M}_{g,1}, \ldots, \tilde{M}_{g,F_g}$ of a given multi-channel image $\tilde{M}_g$ should be warped using the same transformation $\boldsymbol{T}_g(\boldsymbol{\mu}_g)$. We therefore incorporate a restricted transformation model within the standard groupwise registration approach of Equation (4). The new optimisation problem that we propose to solve is:

$$\begin{aligned}\hat{\boldsymbol{\mu}} = \arg\min_{\boldsymbol{\mu}} \mathcal{D}(&\tilde{M}_{1,1}(\boldsymbol{T}_1(\boldsymbol{\mu}_1)), \ldots, \tilde{M}_{1,F_1}(\boldsymbol{T}_1(\boldsymbol{\mu}_1)), \ldots \\ &\tilde{M}_{g,1}(\boldsymbol{T}_g(\boldsymbol{\mu}_g)), \ldots, \tilde{M}_{g,F_g}(\boldsymbol{T}_g(\boldsymbol{\mu}_g)), \ldots \\ &\tilde{M}_{G,1}(\boldsymbol{T}_G(\boldsymbol{\mu}_G)), \ldots, \tilde{M}_{G,F_G}(\boldsymbol{T}_G(\boldsymbol{\mu}_G)))\end{aligned} \tag{6}$$

This optimisation is subject to Equation (5). In this scheme, image dissimilarity $\mathcal{D}$ is assessed in an analogous way as in the existing groupwise mono-channel registration scheme (see Section II-C), but the different optimisation procedure induces that the images are warped by groups.

This novel groupwise multi-channel image registration scheme allows to take into account correlations between any pair of channel images $\tilde{M}_{g,f}$, and not just the corresponding channels that have the same feature index f, which is a limitation of pairwise multi-channel registration (Equation (2)). In our framework, we consider all $\sum_{g=1}^{G} F_g$ images together. In this way, the information that is shared between any pair of channel images can be taken into account, and not only the information shared between corresponding channels. Moreover, the scheme that we propose can be directly extended to datasets for which different numbers of channels are computed for each multi-channel image: in other words, our method does not suppose that there exists corresponding channel images, computed from each original image.

E. Choice of the Dissimilarity Measure

Multiple intensity-based groupwise dissimilarity metrics have been proposed and could be used within the novel multi-channel registration framework described in section II-D.

A particular case would be that the images of $\tilde{\mathcal{M}}$ are multi-channel and monomodal. In that case, choosing the groupwise dissimilarity measure based on the sum of variances, devised by Metz *et al*. [15] for images with similar intensities, would be appropriate.

In the most general case, however, the $\sum_{g=1}^{G} F_g$ images of $\tilde{\mathcal{M}}$ may have different contrasts. The groupwise dissimilarity measure to choose within the novel scheme should ideally handle such contrast differences. This is the case of the groupwise dissimilarity measures based on principal component analysis developed by Huizinga *et al*. [18], or based on mutual information by Bhatia *et al*. [14] or Guyader *et al*. [20]. The total correlation dissimilarity measure for groupwise registration (denoted $\mathcal{D}_{\mathrm{TC}}$), devised by Guyader *et al*. [20], is one of the multivariate versions of mutual information. Previous studies [20] have shown that total correlation yields equal or better registration results than competing state-of-the-art methods on quantitative MRI datasets. Given the performances of total correlation on such non-monomodal datasets, we made the choice to select it as groupwise dissimilarity measure witin the multi-channel and generic registration framework described in section II-D. This choice of dissimilarity measure was made to apply the novel scheme in a concrete case, but other choices in terms of dissimilarity measures and other registration components could have been made (see Discussion section). The total correlation dissimilarity measure $\mathcal{D}_{\mathrm{TC}}$ is based on the computation of a correlation matrix $\mathbf{K}$ (see supplement material A for details), obtained from the images $M_1, \ldots, M_G$ in the existing groupwise mono-channel registration scheme (see section II-C), and obtained from the channel images $\tilde{M}_1, \ldots, \tilde{M}_G$ in the novel groupwise multi-channel registration scheme that we propose (see section II-D). Total correlation is computed as follows:

$$\mathcal{D}_{\mathrm{TC}} = \frac{1}{2} \sum_{j=1}^{G} \ln \lambda_j \tag{7}$$

with λ_j the jth eigenvalue ($\lambda_j > \lambda_{j+1}$) of the correlation matrix $\mathbf{K}$ based on the image intensities of the images or channel images to register (see supplement material A).

F. Optimisation Methods and Implementation Details

The adaptive stochastic gradient descent (ASGD) of Klein *et al*. [25] was used as optimisation method for solving Equation (6). This method randomly samples positions in the image space at each iteration to reduce computation time. For the ASGD optimisation, the derivative of the cost function has to be computed. To that purpose, we followed the work of van der Aa [26] to differentiate the eigenvalue decomposition, similarly to what Huizinga *et al*. [18] did. Sampling is done off the voxel grid, which was shown to be necessary to reduce interpolation artefacts [27]. We chose to use an Euler parametrisation for rigid transformations (i.e. linear with 3 rotations and 3 translations, without scaling) and a B-spline model for non-rigid (i.e. non-linear) transformations.

A multi-resolution strategy was used: the images are Gaussian-blurred with a certain standard deviation, which is decreased at each resolution level. With this procedure, the large deformations are corrected first, and the finer deformations are corrected in subsequent levels. Linear interpolation is used to interpolate the images during registration, which reduces computation time without significantly compromising registration accuracy [18], but cubic B-spline interpolation was used to produce the final registered images.

The registration framework that we propose supports the inclusion of regularisation terms in a trivial way [27]. However, we chose to leave these considerations out of the present work, to avoid the introduction of another hyperparameter (weight of the regularisation term). Instead, we keep the B-spline control point (when applicable) rather conservative, which intrinsically already provides some regularisation.

Many other choices for rigid (e.g. [28], [29]) and non-rigid (e.g. [1], [22], [30]–[34]) transformation models exist and could have been used in this study, but also when it comes to the different optimisation methods (e.g. gradient descent [35], quasi-Newton [36], nonlinear conjugate gradient [37], Kiefer–Wolfowitz [38], simultaneous perturbation [39], Robbins–Monro [40], and evolution strategy [41]), different groupwise dissimilarity measures (see section II-C), multi-resolution strategies [42], and different regularisation terms (e.g. [43]–[45]). Comparing these different methods exhaustively is outside the scope of this paper: what we propose in this article is a generic framework that can be customised for different applications.

III. Experiments

The groupwise multi-channel registration scheme presented in section II-D was evaluated on two multimodal imaging datasets, and compared to three other registration scenarios.

A. Registration Scenarios

Four registration scenarios are compared. Each of them is detailed in this section and illustrated in Fig. 1.

1) Scenario A: Groupwise Multi-Channel Image Registration: This scenario uses the novel groupwise multi-channel scheme introduced in section II-D, Equation (6). The feature images that we use are the modality independent neighbourhood descriptors (MIND) introduced by Heinrich *et al*. [6]. MIND feature images are obtained based on local variance and patch-based distances, using the following expression:

$$\tilde{M}_{g,f}(\boldsymbol{x}) = \frac{1}{n} \exp\left(-\frac{D_p(M_g, \boldsymbol{x}, \boldsymbol{x} + \boldsymbol{r}_f)}{V(M_g, \boldsymbol{x})}\right) \tag{8}$$

where D_p is a patch-based distance, V an estimation of local variance, and n a normalisation constant. F spatial search vectors $\boldsymbol{r}_1, \ldots, \boldsymbol{r}_F$ serve to compute F MIND feature images $\tilde{M}_{g,1}, \ldots, \tilde{M}_{g,F}$ for each original image M_g. For a given vector $\boldsymbol{r}_f$, the MIND images obtained from different original images $\tilde{M}_{1,f}, \ldots, \tilde{M}_{G,f}$ have a quite similar appearance [6], [46], as shown in Fig. 2. However, this is not the case when different $\boldsymbol{r}_f$ are considered. As justified in section II-E, total correlation $\mathcal{D}_{\mathrm{TC}}$ is taken as groupwise dissimilarity measure in that scenario.

2) Scenario B: Pairwise Multi-Channel Image Registration: In this second scenario, we use the existing pairwise multi-channel scheme described in Equation (3). MIND feature images are used, like in scenario A, to build the multi-channel set of images that has to be registered. MIND feature images obtained for a given index f have similar intensity distributions, irrespective of the modality of the original image. The pairwise multi-channel dissimilarity measure that we choose to consider in this scenario is mutual information $\mathcal{D}_{\mathrm{MI}}$ [21], [28]:

$$\mathcal{D}_{\mathrm{PMC}}(\tilde{\mathcal{M}}) = \sum_{f=1}^{F} \mathcal{D}_{\mathrm{MI}}\left(\tilde{M}_{1,f}, \tilde{M}_{2,f}\right) \tag{9}$$

with M_a, M_b two images with N samples.

3) Scenario C: Groupwise Mono-Channel Registration: Scenario C consists of applying existing groupwise mono-channel registration to the original images, without using any feature image. The registration scheme is the one corresponding to Equation (4), using $\mathcal{D}_{\mathrm{TC}}$ as dissimilarity measure.

4) Scenario D: Pairwise Mono-Channel Registration: In scenario D, we apply pairwise mono-channel registration based on mutual information $\mathcal{D}_{\mathrm{MI}}$ to the original images.

5) Additional Groupwise Scenarios: To provide insight into the influence of the choice of the groupwise dissimilarity measure, experiments similar to scenario A and C were repeated, but with another dissimilarity measure than $\mathcal{D}_{\mathrm{TC}}$. Huizinga *et al*. [18] previously designed a groupwise dissimilarity measure based on principal component analysis, denoted $\mathcal{D}_{\mathrm{PCA2}}$, the expression of which is close to $\mathcal{D}_{\mathrm{TC}}$. In their study, Huizinga *et al*. [18] concluded that the registration results obtained with $\mathcal{D}_{\mathrm{PCA2}}$ were similar to or better than results obtained with other state-of-the-art techniques, which is why we also performed results with that dissimilarity measure. We additionally performed the same experiments with Wachinger and Navab's [17] dissimilarity measure based on accumulated pairwise estimates, $\mathcal{D}_{\mathrm{APE}}$, which is not based on mutual information and not closely related to $\mathcal{D}_{\mathrm{TC}}$.

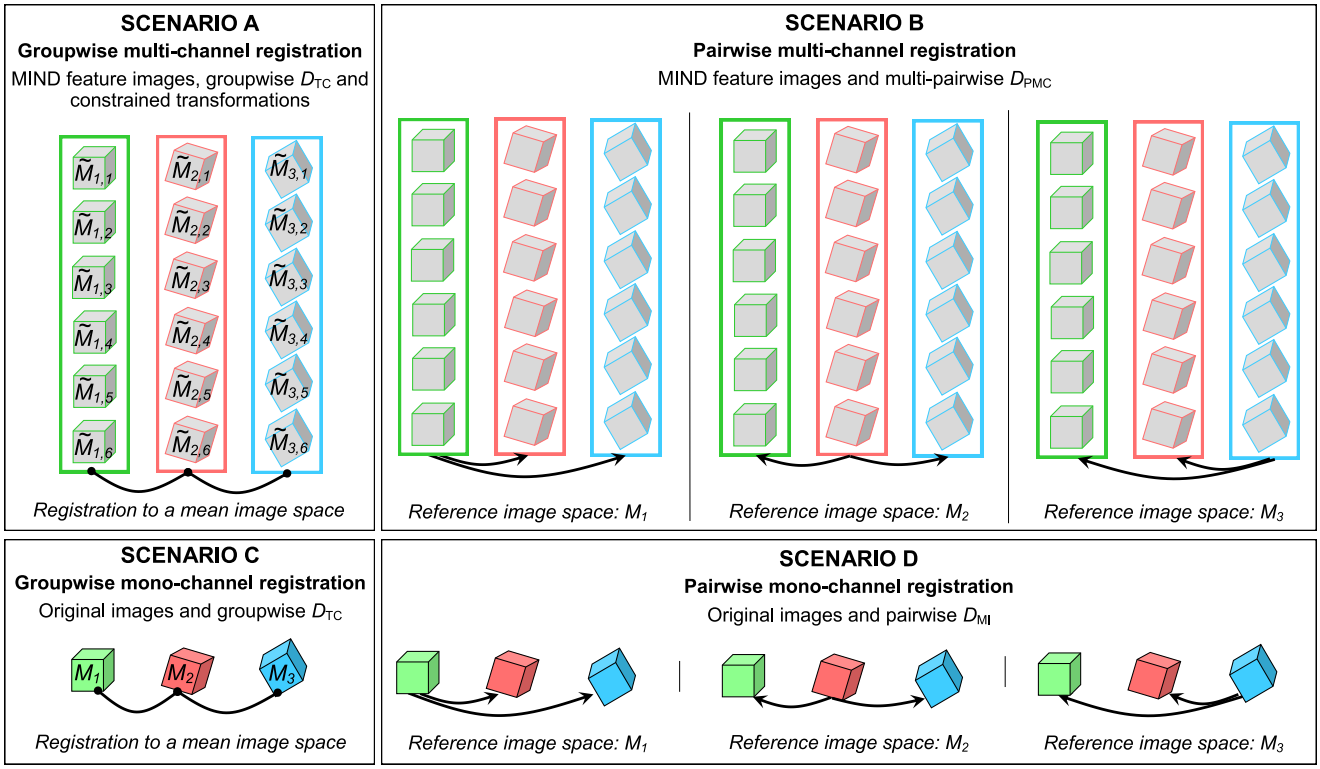

Fig. 1. Registration scenarios (case with 3 original images).

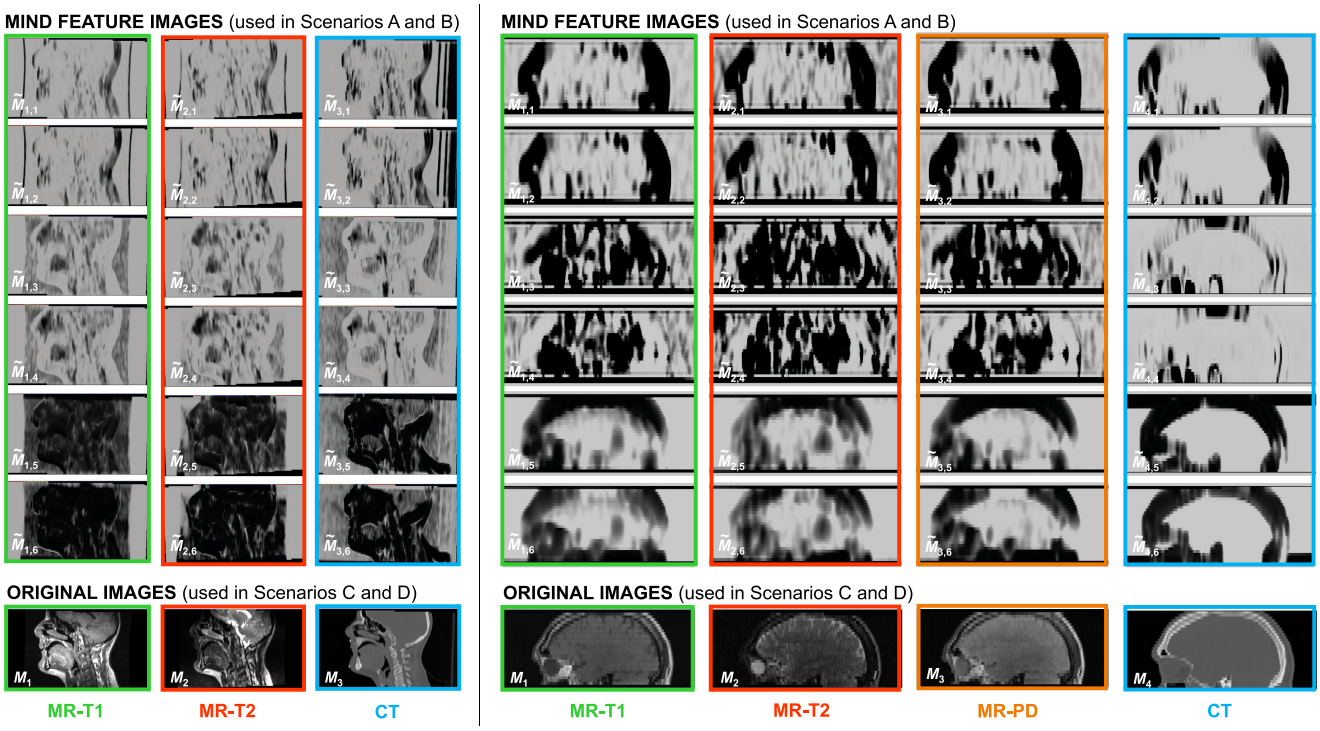

Fig. 2. Examples of MIND feature images and original images for the head and neck dataset and for the RIRE dataset. (a) Head and neck dataset. (b) RIRE dataset.

B. Experiment 1: Head and Neck Multimodal Dataset

Twenty-two patients with a tumour in the head and neck region [47]–[50] were scanned for radiotherapy and hyperthermia treatment planning [51], [52]. Approval was obtained from the institutional review board in regard to our study (number: METC-2010-318). A multimodal dataset was acquired for each patient, consisting of a T1-weighted magnetic resonance image (MRI), a T2-weighted MRI, and a computed tomography (CT) image. The CT images were acquired using a Siemens scanner (Somatom Sensation Open, Siemens), with a voxel size of $0.98 \times 0.98 \times 2.50\,\text{mm}^3$ for 21 patients, and $1.27 \times 1.27 \times 2.50\,\text{mm}^3$ for the remaining patient. The T1 and T2-weighted MR images were acquired on a 1.5 T scanner (Optima MR450w, General Electric Healthcare). Half of the patients had MR images with a voxel size of $0.49 \times 0.49 \times 3.00\,\text{mm}^3$, the other half of $0.68 \times 0.68 \times 3.00\,\text{mm}^3$. The out-of-plane field of view (FOV) was 20 cm centered at the location of the tumour, yielding slightly different FOV values among patients. T1 and T2 images were corrected for intensity inhomogeneity, using the N3 method [53] for the T1 images, and the built-in algorithm (surface coil intensity correction) of the MR scanner for the T2 images. Radiotherapy immobilisation masks were used [48] both for the acquisition of the MR and CT images. For 12 patients (subset α), the immobilisation masks covered the head, the neck and the shoulders. For this first subset, the MR images were acquired using 6-channel flex coils allowing for the same immobilisation position in both the MR and CT acquisitions. For the remaining ten patients (subset β), smaller immobilisation masks were used, covering only the anterior parts of the head and neck region. For this second subset, the use of head coils made it impossible to impose the exact same patient position in the CT and MR acquisitions.

1) Image Preparation: In the current implementation of the method, the groupwise multi-channel and mono-channel schemes operate provided that the images to register have equal voxel sizes. To ensure that this is the case, the T2 and CT images were first coarsely registered to the T1 image using a rigid transformation and pairwise mutual information. The images were subsequently misaligned using artificially generated Euler transformations. The data was resampled only once for these operations. These transformations were randomly generated using uniform distributions (translations ± 10 mm, rotations ± 0.25 rad). To generate the MIND feature images, we chose a Gaussian weighting of $\sigma = 2$, and a six-neighbourhood spatial region for the search vectors $\boldsymbol{r}_1, \ldots, \boldsymbol{r}_F$, resulting in $F = 6$ feature images for each acquired image [6], [46]. Examples of such images are shown in Fig. 2(a).

2) Registration Settings: For each patient, the original images after image preparation are denoted M_1 (the T1-weighted MRI), M_2 (the T2-weighted MRI) and M_3 (the CT image).

The four image registration scenarios described in section III-A. are then applied to the image datasets. Registrations were applied in two consecutive steps. Firstly, with a rigid transformation model based on Euler transformations, and secondly with a deformable model based on B-spline transformations [22] with control point spacing of 100 mm, to account for possible non-rigid misalignments due to different patient bulk positioning or organ positioning (especially in the neck region) between the scans. The Euler transformations were taken as starting points for the registrations based on B-splines. Initial trial-and-error experiments suggested that the value of 100 mm is sufficient to compensate for the deformations in the head and neck images. Three resolutions of 1000 iterations each with a smoothing σ of 8, 4 and 2 voxels were used in both the Euler and B-spline cases. For the pairwise mono-channel registrations based on mutual information, the number of bins that we selected was 32. A B-spline Parzen windowing approach was used to estimate the probability density function for mutual information [54]. Furthermore, registration masks for the head and neck region were delineated for each patient for all modalities in order to prevent the influence on registration of artefacts such as ghosting for the MR images, and the presence of the immobilisation. Considering that these feature images show noisy backgrounds, these registration masks seemed to be particularly necessary when MIND images have to be registered (Fig. 2).

3) Registration Evaluation: For each patient, an expert placed $n = 19 \pm 2$ corresponding landmarks for all imaging modalities. Registration accuracy was evaluated by computing the following target registration error (TRE) between the landmarks of the three modalities:

$$\text{TRE} = \frac{1}{3}\left(d_{\text{T1}-\text{T2}} + d_{\text{T1}-\text{CT}} + d_{\text{T2}-\text{CT}}\right) \quad \text{with} \quad d_{\boldsymbol{p}-\boldsymbol{q}} = \frac{1}{n}\sum_{i=1}^{n} ||\boldsymbol{p}_i - \boldsymbol{q}_i|| \tag{10}$$

with $\boldsymbol{p}_i$ and $\boldsymbol{q}_i$ the landmark coordinates, $||\,.\,||$ the Euclidean distance, and $d_{\boldsymbol{p}-\boldsymbol{q}}$ the average landmark distance between the modalities $\boldsymbol{p}$ and $\boldsymbol{q}$. The head and neck dataset allows to study the influence of the choice of reference image: T1, T2 or CT. In the pairwise multi-channel case (scenario B) and in the pairwise mono-channel case (scenario D), the landmarks were directly propagated to the three image reference spaces of T1, T2 and CT. In the groupwise cases (scenarios A and C), no reference space is chosen during registration (all images are brought to an average space), but the evaluation of registration accuracy can be done in the image spaces of the original images. To that purpose, the landmarks were brought to the average image space, and were subsequently propagated to each of the original image spaces T1, T2 or CT by using the inverses of the transformations obtained by the groupwise registrations [15]. Wilcoxon signed-rank tests were used to assess significance of comparisons of TRE values with respect to scenario A. Significance was considered for $p < 0.01$. Intra-rater variability (IRV) was assessed by repeating the placement of landmarks one month after the first placement session. This operation was done for the T2 and CT images before the artificial misalignments were applied. Landmarks were not annotated on T1 because of the natural alignment of the T1 and T2 images at the moment of acquisition. For each patient, the IRV was computed using $\text{IRV} = \frac{1}{2}\left(d_{\text{T2}-\text{T2}^\diamond} + d_{\text{CT}-\text{CT}^\diamond}\right)$, the $\diamond$ referring to the second session of landmark delineation.

C. Experiment 2: RIRE Multimodal Dataset

This experiment focuses on multimodal images of the publicly available Retrospective image registration evaluation (RIRE) project [29]. Out of the 18 patient datasets available on the website of the RIRE project (http://www.insight-journal.org/rire/), we selected the 12 datasets including at least the three following modalities: CT, MR-T1 and MR-T2. Seven of these 12 datasets also included a proton density-weighted MR image (MR-PD). PET images were not considered in this study because of the presence of halo artefacts. CT images had a voxel size between $0.40 \times 0.40 \times 3.00\,\mathrm{mm}^3$ and $0.65 \times 0.65 \times 4.00\,\mathrm{mm}^3$, and MR images had a voxel size between $0.82 \times 0.82 \times 3.00\,\mathrm{mm}^3$ and $1.25 \times 1.25 \times 4.00\,\mathrm{mm}^3$. One of the patients was not included because the field of view of the MRIs was much smaller than for the CT image.

1) Image Preparation: The initial step was to resample the T1, T2 and PD images (when present) to the image space of the CT image. MIND images are computed using the same settings as described in section III-B1. Examples of such images are shown in Fig. 2(b).

2) Registration Settings: The registration scenarios that we considered are the same as for Experiment 1. Only the CT image was taken as fixed reference space in scenarios B and D due to the specific requirements of the online evaluation tool. Registrations were applied in two consecutive steps. Firstly, with a translation transformation model, and secondly with an Euler transformation model. The translation transformations were taken as starting points for the registrations based on Euler. Non-rigid transformations were not considered for RIRE datasets, following the guidelines of the RIRE online platform. In a similar fashion to the head and neck dataset, registration masks were used to exclude the background during registration. The registration parameters that were used here are identical to those of Experiment 1.

3) Registration Evaluation: The registrations were evaluated by uploading lists of points to the website of the RIRE project. The ground truth is made available in an indirect manner only: users cannot get direct access to the ground truth, and instead have to upload points transformed using the registration results. In contrast to the head and neck dataset, the ground truth is here only known with respect to the CT images, which is why the influence of the choice of reference image could not be studied in the framework of this experiment. Wilcoxon signed-rank test were used to assess significance of comparisons of TRE values with respect to scenario A.

D. Experiment 3: Groupwise Multi-Channel Registration for Multi-Channel Images With Different Numbers of Channels

As mentioned in the Method section, the groupwise multi-channel scheme described in this article offers the possibility to register datasets of multi-channel images with different numbers of channels. For the head and neck dataset, we performed an example of a groupwise multi-channel registration with total correlation $\mathcal{D}_{\mathrm{TC}}$ with all MIND channels for T1 ($\tilde{M}_{1,1}, \ldots, \tilde{M}_{1,6}$), with 4 MIND channels for T2 ($\tilde{M}_{2,1}, \ldots, \tilde{M}_{2,4}$), and with 5 MIND channels for CT ($\tilde{M}_{3,1}, \ldots, \tilde{M}_{3,5}$). The registration settings are the same as those described in Experiment 1 (section III-B2).

TABLE I
EXPERIMENT 1 – TRE [MM] FOR EACH REFERENCE SPACE T1, T2, AND CT

			Ⓐ Groupwise multi-channel			Ⓑ Pairwise multi-channel			Ⓒ Groupwise mono-channel			Ⓓ Pairwise mono-channel			
	Patient	Mis.	T1	T2	CT	T1	T2	CT	T1	T2	CT	T1	T2	CT	IRV
α : Large radiotherapy mask	1	24.7	2.2	2.2	2.2	2.2	2.1	2.1	106.8	113.1	108.2	1.7	2.0	2.4	0.8
	2	14.9	2.3	2.3	2.2	2.1	2.2	2.1	101.9	110.8	105.0	2.1	2.2	2.6	1.1
	3	22.2	2.0	2.0	2.0	1.7	2.0	1.7	8.4	8.3	9.4	1.7	1.7	2.0	0.8
	4	22.9	2.3	2.3	2.3	1.9	2.2	2.2	115.8	112.8	126.7	1.9	2.2	2.6	0.8
	5	15.8	2.6	2.6	2.6	2.4	2.3	2.5	8.2	8.3	8.2	2.5	2.5	3.6	0.8
	6	17.2	2.5	2.5	2.5	2.3	2.4	2.4	97.2	99.4	97.6	2.3	2.3	3.2	0.9
	7	21.9	2.0	2.0	2.0	2.1	1.8	1.9	11.0	10.8	12.2	1.8	2.0	2.4	0.8
	8	18.5	2.1	2.1	2.1	2.0	2.0	2.1	25.2	25.1	25.1	1.9	2.1	3.0	0.8
	9	19.9	1.9	1.9	1.9	1.7	1.8	1.9	94.0	108.1	108.6	1.6	1.7	2.5	1.1
	10	19.3	2.4	2.4	2.3	2.2	2.1	2.1	107.0	109.7	102.3	2.2	2.0	2.8	0.8
	11	15.3	2.5	2.5	2.5	3.5	3.0	2.4	123.0	135.5	124.6	3.4	2.4	2.3	1.1
	12	19.8	2.3	2.2	2.2	2.2	2.5	2.2	65.5	62.7	61.8	2.4	1.9	3.4	1.0
β : Small radiotherapy mask	13	26.4	5.2	5.2	5.0	4.2	3.7	4.5	10.1	10.0	10.6	4.0	4.9	4.7	1.1
	14	21.7	2.7	2.7	2.7	2.5	2.7	2.9	12.1	12.1	12.8	2.6	2.6	2.8	0.8
	15	19.9	2.7	2.7	2.7	2.5	2.5	2.6	6.5	6.4	6.2	2.7	2.9	3.1	0.7
	16	23.3	3.4	3.4	3.4	2.4	3.0	2.9	9.0	9.1	8.7	2.8	3.0	4.0	0.7
	17	16.3	3.8	3.8	3.9	3.3	3.9	3.5	7.3	7.3	7.1	4.3	4.7	5.2	1.1
	18	15.3	4.0	4.0	4.1	4.0	3.7	4.1	10.2	10.0	11.0	4.2	4.4	5.2	0.9
	19	10.9	3.3	3.3	3.4	2.9	3.2	3.6	14.8	14.8	14.8	3.9	4.4	6.1	1.1
	20	22.5	2.5	2.5	2.5	1.8	2.2	2.2	41.9	42.0	38.9	1.8	1.8	12.7	1.1
	21	20.7	3.1	3.1	3.2	3.2	3.1	3.3	19.5	19.5	19.0	2.6	2.9	2.9	0.9
	22	21.1	3.2	3.2	3.2	2.7	2.7	2.6	4.8	4.8	5.0	2.9	3.4	3.1	1.2
Average 1		**19.6**	2.8	2.8	2.8	**2.5**	**2.6**	**2.6**	**45.5**	**47.3**	**46.5**	2.6	2.7	**3.8**	0.9
STD 1		3.6	0.8	0.8	0.8	0.7	0.6	0.7	44.0	46.8	45.7	0.8	1.0	2.2	0.2
Variability		-	7×10^{-3}			3×10^{-2}			0.8			0.5			-
Average 2		**19.6**	2.8			**2.6**			**46.4**			3.0			0.9
STD 2		3.6	0.8			0.7			45.5			1.6			0.2

Bold values of Average 1 and Average 2 signal distributions that are significantly different from scenario A (underlined values). For Average 1, the comparisons were performed per reference space. For Average 2, all data was considered together.

E. Implementation

All registration methods used in this study were implemented as part of the open source package elastix [27]. For the experiments, image manipulations were performed using Python (version 2.7.3) with packages NumPy 1.6.2, SciPy 0.11.0, pydicom 0.9.7, and NiBabel 1.3.0. To obtain the MIND feature images, we directly used the MATLAB code made available by its authors (http://www.ibme.ox.ac.uk/research/biomedia/julia-schnabel/Software). All computations were done on a Linux machine (64 GB of memory, 8 cores, 2412 MHz).

IV. RESULTS

A. Results on Experiment 1: Head and Neck Dataset

Target registration errors (TRE) obtained for the head and neck dataset are presented in Table I for the four registration scenarios and for the three reference spaces T1, T2 and CT. Results obtained for the groupwise scenarios with $\mathcal{D}_{\mathrm{PCA2}}$ and $\mathcal{D}_{\mathrm{APE}}$ are presented in supplement material B. *Average 1* and *STD 1* are obtained based on the TRE values that correspond to a given scenario and a given reference space. *Average 2* and *STD 2* are obtained based on all TRE values for a given scenario.

Focusing first on the *Average 2* values, it is observed that scenario C resulted in gross registration failures, which was the case with $\mathcal{D}_{\mathrm{TC}}$, with $\mathcal{D}_{\mathrm{PCA2}}$ and with $\mathcal{D}_{\mathrm{APE}}$. The lowest registration errors were obtained with scenario B, which was significantly lower than for scenarios A and D. Similar patterns are observed when focusing on *Average 1* values. A discordant

TABLE II
EXPERIMENT 2 – TRE [MM]

Patient	Misaligned case	Ⓐ Groupwise multi-channel	Ⓑ Pairwise multi-channel	Ⓒ Groupwise mono-channel	Ⓓ Pairwise mono-channel
001	25.1	2.6	2.1	12.9	4.1
002	36.1	1.1	3.3	33.3	3.1
005	38.9	2.3	8.9	16.6	2.5
006	41.0	2.5	12.9	10.6	6.8
007	25.1	1.6	5.9	7.3	2.9
101	14.6	4.7	1.9	58.0	2.5
102	11.6	2.9	2.6	15.2	2.0
105	28.1	7.5	4.5	78.5	8.6
106	23.3	5.8	3.9	6.2	2.3
107	20.9	2.3	2.7	4.7	1.5
108	27.6	3.9	2.8	69.6	1.9
109	27.2	2.3	2.7	85.8	1.7
Average	**26.6**	3.3	**4.3**	**33.2**	3.3
STD	8.5	1.8	3.1	29.6	2.1

Bold values signal distributions that are significantly different from scenario A (underlined values).

note is the fact that the *Average 1* TRE values for scenario D with CT as reference image were substantially larger than the TRE values with the T1 and T2 as reference images. In addition, the difference in *Average 1* TRE values between scenario A and D with CT as reference image was statistically significant.

Comparing the TRE values between the reference spaces T1, T2 and CT allows to assess the influence of the choice of reference image on registration accuracy. Standard deviation values were therefore computed between the three average TRE values obtained in each image reference space to measure the registration consistency across the three reference spaces (see Section III-B3). These standard deviations are denoted *Variability* in Table I, and are computed based on the three corresponding values of *Average 1*. The lowest variability was obtained for scenario A. When inspecting the individual TRE values for each subject, this becomes even more apparent.

Table I clearly indicates that the TRE values obtained for subset α (large immobilisation mask) are lower than for subset β (small immobilisation mask). This result can be explained by the fact that the immobilisation mask and gradient coils used for subset β did not allow a similar positioning of the patient between the CT and MR acquisitions. In particular, rotations of the neck region may make the registration more challenging. The intra-rater variability averaged over all patients is 0.9 mm, which is about three times lower than the best *Average 2* TRE.

B. Results on Experiment 2: RIRE Dataset

For the RIRE dataset, the registration accuracy results are presented in Table II. Results obtained for the additional scenarios with $\mathcal{D}_{\mathrm{PCA2}}$ and $\mathcal{D}_{\mathrm{APE}}$ are presented in supplement material B. The average TRE before registration is 26.6 mm. After registration, the average TRE is 3.3 mm for scenario A, 4.3 mm for scenario B, 33.2 mm for scenario C and 3.3 mm for scenario D. Contrary to Experiment 1, the best registration results were here obtained with groupwise multi-channel registration (scenario A), and with pairwise mono-channel registration (scenario D).

C. Results on Experiment 3: Groupwise Multi-Channel Registration for Multi-Channel Images With Different Numbers of Channels

In this experiment, we considered the images obtained from patients 1 to 12 of the head and neck dataset. Using the set of images $\{\tilde{M}_{1,1}, \ldots, \tilde{M}_{1,6}, \tilde{M}_{2,1}, \ldots, \tilde{M}_{2,4}, \tilde{M}_{3,1}, \ldots, \tilde{M}_{3,5}\}$, which includes different numbers of channels for each multi-channel image, we obtained an average TRE of 2.3 mm, which is only slightly worse than the TRE of 2.2 mm obtained in the original experiment with all channels.

V. DISCUSSION

In this study, we presented a novel groupwise multi-channel image registration scheme. This scheme can be combined with a wide range of groupwise dissimilarity measures and sets of feature images. As a proof of concept, we applied this groupwise multi-channel registration scheme to MIND feature images, and used total correlation $\mathcal{D}_{\mathrm{TC}}$ as groupwise dissimilarity measure.

Groupwise multi-channel image registration (scenario A) was compared to a pairwise multi-channel registration scheme (scenario B). The first main theoretical advantage of the groupwise multi-channel scheme is that it is fully symmetric, and therefore has transitive consistency by definition. Additionally, groupwise multi-channel image registration is directly extensible to datasets for which different numbers of feature images are computed for each image, which is not the case for the pairwise multi-channel dissimilarity measure. Results on two multimodal datasets (head and neck and RIRE) indicate that groupwise multi-channel registration achieves similar registration accuracy as pairwise multi-channel registration, in terms of TRE (scenario A yielded better TRE results than scenario B for the RIRE dataset, but slightly worse for the head and neck dataset). In terms of variability, the experiments on the head and neck dataset confirm the interest of the symmetric groupwise formulation, in the sense that TRE results depend more on the reference space in the pairwise methods than in the groupwise multi-channel approach. The poor variability figures obtained in the groupwise mono-channel case is attributed to the complete registration failure obtained in that case.

These two multi-channel schemes (scenarios A and B) were also compared to mono-channel scenarios based on the original images only, either in a groupwise manner (scenario C), or in a pairwise manner (scenario D). The fact that scenario C results in a registration failure, while scenario A did not, illustrates the potential of the novel scheme that we propose. The results indicate that even when groupwise mono-channel registration with a given dissimilarity measure results in registration failure, there is a possibility to improve the registration results by computing appropriate feature images from the original images (e.g. using MIND feature images) and applying the proposed groupwise

multi-channel registration with the same dissimilarity measure. Besides, the experiment on the head and neck dataset indicates that groupwise multi-channel registration (scenario A) is much less sensitive towards the choice of reference space than pairwise mono-channel registration (scenario D), which verifies one of the advantages of groupwise registration with respect to pairwise registration.

Groupwise total correlation was previously applied to monomodal and quantitative MR images and did not require the use of feature images to obtain results similar or better than pairwise mutual information [18], [55]. The fact that the groupwise total correlation dissimilarity measure requires feature images like MIND images for the registration of multimodal datasets might be explained by the fact that such feature images are more similar to one another, and therefore easier to register (which indeed was the prime motivation for developing MIND [6]). The approximation of total correlation used for the sake of computational feasibility are apparently too drastic in the case of true multimodal images, while it worked on multi-parametric images as shown in [20]. MIND pre-processing allows to make the images sufficiently similar so that they can be registered using total correlation.

The focus of our study was to present a novel multi-channel groupwise registration technique, and does not consist of a comparison between multiple pre-processing algorithms. However, many other pre-processing methods, like ALOST [56] could have been tested. Many choices would have been possible with respect to the transformation model, regularisation, optimisation, pre-processing features and dissimilarity measures (see Section II-F), in particular. Comparing various such components is outside of the scope of this paper. Our key contribution, i.e. the formulation of multi-channel image registration as a groupwise registration problem, is independent of these choices. We do not claim that the proposed groupwise multi-channel method is per se better than mono-channel registration. Some dissimilarity measures might be better in coping with certain differences in intensities than others, and it depends on the image characteristics which dissimilarity measure is optimal. For pairwise registration, mutual information is a proven robust method that works in many multimodal registration scenarios. Yet, it was shown that using additional features yields improved performances in certain applications [3], [5], [6]. For groupwise situations, no analogous approach to mutual information has been presented yet, so there the use of multiple feature channels, as proposed in our study, is a worthwhile option to consider. However, we cannot claim that this multi-channel approach will lead *in general* to better performance.

VI. Conclusion

In this article, we described a scheme for the groupwise registration of multi-channel images. We showed that the registration of multiple sets of feature images can be solved effectively with a groupwise multi-channel registration method, using previously proposed intensity dissimilarity measures suitable for multiparametric imaging data, in combination with a restricted transformation model that assigns a single transformation to all feature images that belong together. In this way, the shared information between all feature images of all images is taken into account, the number of feature images in each set is flexible, the registration is unbiased (i.e. there is no need to choose a reference frame), and the approach naturally scales to scenarios with more than two sets of feature images.

References

[1] G. K. Rohde, S. Pajevic, C. Pierpaoli, and P. J. Basser, "A comprehensive approach for multi-channel image registration," in *Proc. Biomed. Image Registration*, 2003, pp. 214–223.

[2] G. K. Rohde, S. Pajevic, and C. Pierpaoli, "Multi-channel registration of diffusion tensor images using directional information," in *Proc. IEEE Int. Symp. Biomed. Imag.*, 2004, pp. 712–715.

[3] P. A. Legg, P. L. Rosin, D. Marshall, and J. E. Morgan, "A robust solution to multi-modal image registration by combining mutual information with multi-scale derivatives," in *Proc. Med. Image Comput. Compu. Assisted Intervention Conf.*, 2009, pp. 616–623.

[4] D. Russakoff, C. Tomasi, T. Rohlfing, C. Maurer, T. Pajdla, and J. Matas, "Image similarity using mutual information of regions," in *Proc. Eur. Conf. Comput. Vis.*, 2004, pp. 596–607.

[5] M. Staring, U. A. van der Heide, S. Klein, M. A. Viergever, and J. P. W. Pluim, "Registration of cervical MRI using multifeature mutual information," *IEEE Trans. Med. Imag.*, vol. 28, no. 9, pp. 1412–1421, Sep. 2009.

[6] M. P. Heinrich *et al.*, "MIND: Modality independent neighbourhood descriptor for multi-modal deformable registration," *Med. Image Anal.*, vol. 16, no. 7, pp. 1423–1435, 2012.

[7] Z. Li, D. Mahapatra, J. Tielbeek, J. Stoker, L. van Vliet, and F. Vos, "Image registration based on autocorrelation of local structure," *IEEE Trans. Med. Imag.*, vol. 35, no. 1, pp. 63–75, Jan. 2016.

[8] R. O. Suarez, O. Commowick, S. P. Prabhu, and S. K. Warfield, "Automated delineation of white matter fiber tracts with a multiple region-of-interest approach," *NeuroImage*, vol. 59, no. 4, pp. 3690–3700, 2012.

[9] M. P. Heinrich, B. W. Papiez, J. A. Schnabel, and H. Handels, "Multispectral image registration based on local canonical correlation analysis," in *Proc. Med. Image Comput. Comput. Assisted Intervention*, 2014, vol. 17, pp. 202–209.

[10] M. Chen, A. Carass, A. Jog, J. Lee, S. Roy, and J. L. Prince, "Cross contrast multi-channel image registration using image synthesis for MR brain images," *Med. Image Anal.*, vol. 36, pp. 2–14, 2017.

[11] X. Geng, G. E. Christensen, H. Gu, T. J. Ross, and Y. Yang, "Implicit reference-based group-wise image registration and its application to structural and functional MRI," *NeuroImage*, vol. 47, no. 4, pp. 1341–1351, 2009.

[12] S. Joshi, B. Davis, M. Jomier, and G. Gerig, "Unbiased diffeomorphic atlas construction for computational anatomy," *NeuroImage*, vol. 23, no. Suppl. 1, pp. S151–S160, 2004.

[13] E. Learned-Miller, "Data driven image manifolds through continous joint alignment," *IEEE Trans. Pattern Anal.*, vol. 28, no. 2, pp. 236–250, Feb. 2006.

[14] K. K. Bhatia, J. Hajnal, A. Hammers, and D. Rueckert, "Similarity metrics for groupwise non-rigid registration," in *Proc. Med. Image Comput. Comput. Assisted Intervention*, 2007, vol. 2, pp. 544–552.

[15] C. Metz, S. Klein, M. Schaap, T. van Walsum, and W. Niessen, "Nonrigid registration of dynamic medical imaging data using nD + t B-splines and a groupwise optimization approach," *Med. Image Anal.*, vol. 15, no. 2, pp. 238–249, 2011.

[16] Z. Špiclin, B. Likar, and F. Pernuš, "Groupwise registration of multimodal images by an efficient joint entropy minimization scheme," *IEEE Trans. Med. Imag.*, vol. 21, no. 5, pp. 2546–2558, May 2012.

[17] C. Wachinger and N. Navab, "Simultaneous registration of multiple images: Similarity metrics and efficient optimization," *IEEE Trans. Pattern Anal.Mach. Intell.*, vol. 35, no. 5, pp. 1221–1233, May 2013.

[18] W. Huizinga, D. H. J. Poot, J. Guyader, R. Klaassen, B. F. Coolen, and M. V. Kranenburg, "PCA-based groupwise image registration for quantitative MRI," *Med. Image Anal.*, vol. 29, pp. 65–78, 2016.

[19] M. Polfliet, W. Huizinga, S. Klein, and J. D. Mey, "Pythagorean mean images for efficient groupwise registration," in *Proc. Med. Image Comput. Compu. Assisted Intervention Conf. Imag. Comput. Assistance Radiation Therapy Workshop*, 2015, pp. 26–33.

[20] J.-M. Guyader *et al.*, "Total correlation-based groupwise image registration for quantitative MRI," in *Proc. Int. Workshop Biomed. Image Registration*, 2016, pp. 186–193.

[21] J. Pluim, J. Maintz, and M. Viergever, "Mutual information based registration of medical images: A survey," *IEEE Trans. Med. Imag.*, vol. 22, no. 8, pp. 986–1004, Aug. 2003.
[22] D. Rueckert, L. I. Sonoda, C. Hayes, D. L. Hill, M. O. Leach, and D. J. Hawkes, "Nonrigid registration using free-form deformations: Application to breast MR images," *IEEE Trans. Med. Imag.*, vol. 18, no. 8, pp. 712–721, Aug. 1999.
[23] J. L. R. Andersson and S. Skare, "A model-based method for retrospective correction of geometric distortions in diffusion-weighted EPI," *Neuroimage*, vol. 16, no. 1, pp. 177–199, 2002.
[24] S. Balci, P. Golland, M. Shenton, and M. Wells, "Free-form B-spline deformation model for groupwise registration," in *Proc. Med. Image Comput. Compu. Assisted Intervention Conf. Statist. Registration Workshop*, 2007, pp. 23–30.
[25] S. Klein, J. Pluim, M. Staring, and M. Viergever, "Adaptive stochastic gradient descent optimisation for image registration," *Int. J. Comput. Vis.*, vol. 81, no. 3, pp. 227–239, 2009.
[26] N. van der Aa, H. G. Ter Morsche, and R. R. M. Mattheij, "Computation of eigenvalue and eigenvector derivatives for a general complex-valued eigensystem," *Electron. J. Linear Al*, vol. 16, pp. 300–314, 2007.
[27] S. Klein, M. Staring, K. Murphy, M. Viergever, and J. Pluim, "Elastix: A toolbox for intensity-based medical image registration," *IEEE Trans. Med. Imag.*, vol. 29, no. 1, pp. 196–205, Jan. 2010.
[28] P. Viola and W. Wells, "Alignment by maximization of mutual information," *Int. J. Comput. Vis.*, vol. 24, no. 2, pp. 137–154, 1997.
[29] J. West, J. Fitwpatrick, M. Wang, and B. Dawant, "Comparison and evaluation of retrospective inter-modality brain image registration techniques," *J. Comput. Assist Tomo*, vol. 21, no. 4, pp. 554–566, 1997.
[30] D. Mattes, D. R. Haynor, H. Vesselle, T. K. Lewellen, and W. Eubank, "PET-CT image registration in the chest using free-form deformations," *IEEE Trans. Med. Imag.*, vol. 22, no. 1, pp. 120–128, Jan. 2003.
[31] F. L. Bookstein, "Principal warps: Thin-plate splines and the decomposition of deformations," *IEEE Trans. Pattern Anal. Mach. Intell.*, vol. 11, no. 6, pp. 567–585, Jun. 1989.
[32] M. H. Davis, A. Khotanzad, D. P. Flamig, and S. E. Harms, "A physics-based coordinate transformation for 3-D image matching," *IEEE Trans. Med. Imag.*, vol. 16, no. 3, pp. 317–328, Jun. 1997.
[33] B. Avants and J. C. Gee, "Geodesic estimation for large deformation anatomical shape averaging and interpolation," *NeuroImage*, vol. 23, pp. S139–S150, 2004.
[34] T. Vercauteren, X. Pennec, A. Perchant, and N. Ayache, "NeuroImage diffeomorphic demons: Efficient non-parametric image registration," *NeuroImage*, vol. 45, no. 1, pp. S61–S72, 2009.
[35] M. Milanič, W. Jia, J. S. Nelson, and B. Majaron, "Numerical optimization of sequential cryogen spray cooling and laser irradiation for improved therapy of port wine stain," *Lasers Surgery Med.*, vol. 43, no. 2, pp. 164–175, 2011.
[36] J. E. Dennis, Jr, J. J. Moré, J. E. Dennis, and J. J. Moré, "Quasi-Newton methods, motivation and theory," *SIAM Rev.*, vol. 19, no. 1, pp. 46–89, 1977.
[37] Y.-H. Dai, "A family of hybrid conjugate gradient methods for unconstrained optimization," *Math Comput.*, vol. 72, no. 243, pp. 1317–1329, 2003.
[38] J. Kiefer and J. Wolfowitz, "Stochastic estimation of the maximum of a regression function," *Ann. Math. Stat*, vol. 23, no. 3, pp. 462–466, 1952.
[39] J. C. Spall, "Multivariate stochastic approximation using a simultaneous perturbation gradient approximation," *IEEE Trans. Autom. Control*, vol. 37, no. 3, pp. 332–341, Mar. 1992.
[40] H. Robbins and S. Monro, "A stochastic approximation method," *Ann. Math. Stat*, vol. 22, no. 3, pp. 400–407, 1951.
[41] N. Hansen and A. Ostermeier, "Completely derandomized self-adaptation in evolution strategies," *Evol. Comput.*, vol. 9, no. 2, pp. 159–195, 2001.
[42] H. Lester and S. R. Arridge, "A survey of hierarchical non-linear medical image registration," *Pattern Recognit.*, vol. 32, no. 1, pp. 129–149, 1999.
[43] M. Staring, S. Klein, and J. P. Pluim, "A rigidity penalty term for nonrigid registration," *Med. Phys.*, vol. 34, no. 11, pp. 4098–4108, 2007.
[44] T. Rohlfing, C. R. Maurer, D. A. Bluemke, and M. A. Jacobs, "Volume-preserving nonrigid registration of MR breast images using free-form deformation with an incompressibility constraint," *IEEE Trans. Med. Imag.*, vol. 22, no. 6, pp. 730–741, Jun. 2003.
[45] B. Fischer and J. Modersitzki, "A unified approach to fast image registration and a new curvature based registration technique," *Linear Algebra Appl.*, vol. 380, pp. 107–124, 2004.
[46] J.-M. Guyader *et al.*, "Groupwise image registration of multimodal head-and-neck images," in *Proc. Int. Symp. Biomed. Imag.*, 2015, pp. 730–733.
[47] V. Fortunati *et al.*, "Feasibility of multimodal deformable registration for head and neck tumor treatment planning," *Int. J. Radiat Oncol*, vol. 90, no. 1, pp. 85–93, 2014.
[48] V. Fortunati *et al.*, "MRI integration into treatment planning of head and neck tumors: Can patient immobilization be avoided?" *Radiother Oncol*, vol. 115, no. 2, pp. 191–194, 2015.
[49] R. F. Verhaart *et al.*, "The relevance of MRI for patient modeling in head and neck hyperthermia treatment planning: A comparison of CT and CT-MRI based tissue segmentation on simulated temperature," *Med. Phys.*, vol. 41, no. 12, 2014, Art. no. 123302.
[50] R. F. Verhaart, V. Fortunati, G. M. Verduijn, T. van Walsum, J. F. Veenland, and M. M. Paulides, "CT-based patient modeling for head and neck hyperthermia treatment planning: Manual versus automatic normal-tissue-segmentation," *Radiother Oncol*, vol. 111, no. 1, pp. 158–163, 2014.
[51] M. Paulides *et al.*, "Simulation techniques in hyperthermia treatment planning," *Int. J. Hyperther*, vol. 29, no. 4, pp. 346–357, 2013.
[52] P. Evans, "Anatomical imaging for radiotherapy," *Phys. Med. Biol.*, vol. 53, no. 12, pp. 151–191, 2008.
[53] J. G. Sled, A. P. Zijdenbos, and A. C. Evans, "A nonparametric method for automatic correction of intensity nonuniformity in MRI data," *IEEE Trans. Med. Imag.*, vol. 17, no. 1, pp. 87–97, Feb. 1998.
[54] P. Thévenaz and M. Unser, "Optimization of mutual information for multiresolution image registration," *IEEE Trans. Med. Imag.*, vol. 9, no. 12, pp. 2083–2099, Dec. 2000.
[55] J.-M. Guyader, L. Bernardin, N. H. Douglas, D. H. Poot, W. J. Niessen, and S. Klein, "Influence of image registration on apparent diffusion coefficient images computed from free-breathing diffusion MR images of the abdomen," *J. Magn. Reson Imag.*, vol. 42, no. 2, pp. 315–330, 2015.
[56] Z. Li, D. Mahapatra, J. A. W. Tielbeek, J. Stoker, L. J. van Vliet, and F. M. Vos, "Image registration based on autocorrelation of local structure," *IEEE Trans. Med. Imag.*, vol. 35, no. 1, pp. 63–75, Jan. 2016.